Dynamic Modeling and Molecular Weight Distribution of Ethylene Copolymerization in an Industrial Gas-Phase Fluidized-Bed Reactor

Mohammad Reza Abbasi[a], Ahmad Shamiri[b,c], Mohamed Azlan Hussain[a*]

[a]Department of Chemical Engineering, Faculty of Engineering, University of Malaya, 50603 Kuala Lumpur, Malaysia

[b]Chemical & Petroleum Engineering Department, Faculty of Engineering, Technology & Built Environment, UCSI University, 56000 Kuala Lumpur, Malaysia

[c]Process System Engineering Center, Faculty of Engineering, Technology & Built Environment, UCSI University, 56000 Kuala Lumpur, Malaysia

[*] Corresponding author. Tel.: +60 379675214, fax: +60 379675319, E-mail address: mohd_azlan@um.edu.my (M.A. Hussain), shamiri@ucsiuniversity.edu.my (A. Shamiri)

Abstract:

A dynamic model for ethylene copolymerization in an industrial fluidized-bed reactor (FBR) is developed to describe its behavior and calculate the properties of polyethylene. The presented model considers particle entrainment and polymerization reaction in two phases. Two-site kinetic and hydrodynamic models in combination, provide a comprehensive model for the gas phase fluidized-bed polyethylene production reactor. The governing moment and hydrodynamic differential equations were solved simultaneously and the results compared with a similar work, as well as industrial data. The dynamic model showed accurate results for predicting Polydispersity Index (PDI), Molecular Weight Distribution (MWD), reactor temperature and polymer production rate.

Keywords: *Polyethylene; Molecular Weight Distribution; Fluidized-Bed Reactor; Dynamic Modeling; Solid Elutriation*

1 Introduction

Olefin polymerization in gas-phase Fluidized-Bed Reactors (FBR) has been recognized as one of the most economic methods of manufacturing commodity polymers including polyethylene (PE), polypropylene (PP) and ethylene-propylene rubber (EPR). Union Carbide, commercialized the first gas-phase fluidized-bed polymerization process, i.e., UNIPOLTM® Process, to produce polyethylene in 1986 [1].

Chemical processes such as gas-solid reactions or gas-phase reactions catalyzed by solids are among the operations which FBRs are utilized extensively. A common use of FBRs in industry is to produce linear low-density polyethylene (LLDPE) by employing heterogeneous Ziegler-Natta (Z-N) catalysts. In contrast to other processes used to produce polyethylene, polymerizing ethylene in a gas-phase FBR have advantages such as better heat removal, operating at decreased temperatures and pressures, and not requiring solvents, which help make it the most broadly used process in industries [2]. Figure 1 shows a typical fluidized-bed polyethylene reactor process flow diagram.

Figure 1: Schematic diagram of an industrial fluidized-bed polyethylene reactor

Fresh feed mixture consisting of ethylene as monomer, 1-butene as co-monomer, hydrogen, and nitrogen is injected from the bottom of the reactor and enters the reaction zone via a distributor. The Z-N catalyst particles are introduced continuously above the distributor to activate the reactants. After fluidization, unreacted gases are separated in the disengagement part of the reactor. Entrained

solids carried by the gas are separated in the cyclone and gets recycled back into the reactor. The reacted gas then passes through the compressor and heat exchanger to be mixed with fresh feed and gets recycled back into the reactor. The product leaves the reactor from just above the distributor and gets collected in a cylinder. Normally, polyethylene producing FBRs available in the industry work within a temperature range of 75–110 ◦C and pressure range of 20–40 bar [3].

The amount of superficial gas velocity (U_0) can be somewhere between 3 to 8 times the minimum fluidization velocity. Various models have been suggested to predict how a gas-phase ethylene polymerization perform in the real world. Researchers have modeled these FBRs as single, two or three phase reactors [4–6]. As a result of assuming that bubbles are free from solids, all of these models considered that reactions occur only in the emulsion phase. Jafari et al. [7] compared the performance of some available models at the time, such as the simple two phase model, dynamic two-phase model and generalized bubbling/turbulent model. They concluded that the bubbling/turbulent model results are better fitted to experimental data in comparison with other approaches.

An overview on modeling different scales available in multiphase chemical reactors such as the heat and mass transfer, kinetics and hydrodynamics was given by Bi and Li [8]. The authors also proposed a Computational Fluid Dynamics (CFD) two fluid model which works towards minimizing energy in single-phase flow. Choi and Ray [4] separated the reactor into two regions of emulsion phase and bubble phase after McAuley et al. [6] regarded the fluidized bed polymerization reactor to be a well-mixed reactor or continuously stirred-tank reactor (CSTR). Fernandes and Lona [9] considered gas in bubble and emulsion phases plus solid polymer particles, all as plug flow phases, to propose their three-phase heterogeneous model. Instead of

considering constant bubble size, Hatzantonis et al. [10] studied the dynamic and steady state behavior of reactor when the bubble size varies. Besides breaking down the reactor into two sections of emulsion phase and bubble phase, they also divided the bubble phase into N well-mixed sections in series and assumed that the emulsion phase is seamlessly mixed. The size of each section in their model, was fixed equivalent to the diameter of the bubble at the relative bed height. Zheng et al. [11] developed a steady-state and dynamic methodology to model the propylene process using the Spheripol Technology. Their kinetic model was based on both single and multisite catalyst and their Molecular Weight Distribution (MWD) results were fitted using the actual Gel Permeation Chromatography (GPC) data. In a similar work, Luo et al. [12] developed a methodology to model the polypropylene process based on Hypol Technology. The authors used Polymer Plus and Aspen Dynamics to predict process behavior and physical properties of the steady-state and dynamic modes.

Meanwhile, some researchers focused on particle size distribution studies in fluidized beds rather than kinetics or property estimation [13–15]. Furthermore, fluidization regimes have also been studied in many works. Different methods to determine fluidization regimes in gas-solid FBRs, such as radioactive particle tracking, electrical capacitance tomography, or magnetic resonance imaging have been applied on these reactors to study different hydrodynamic aspects [16–18]. Alizadeh et al. [2] introduced a pseudo-homogeneous tanks-in-series model to predict the behavior of industrial-scale gas-phase polyethylene production reactor. Kiashemshaki et al. [19] got inspiration from this model and proposed a two-phase model to describe the fluidized bed ethylene polymerization reactor. Their model was a dynamic model except in terms of calculating temperature and comonomer

concentrations. Shamiri et al. [20–22] studied different dynamic modeling and control approaches for gas phase homopolymerization or copolymerization of olefin in FBRs.

In the current study, a fully dynamic modeling approach is used to predict the kinetic and hydrodynamic behavior of industrial polyethylene production reactors and polyethylene properties. The advantage of this model is that it is a two-phase model which considers reaction to take place in both phases. Furthermore, particle elutriation has also been considered in order to take the losses of entrained catalyst and polymer particles from the fluidized bed into account.

A two-site copolymerization kinetic scheme for ethylene and 1-butene were used in this study in order to gain a more realistic picture of copolymerization over a heterogeneous Z-N catalyst in a FBR. Then, the results were compared with a semi-dynamic two-phase model from literature to show the benefits of the current model in comparison to existing models and demonstrate how considering elutriation in ethylene polymerization modeling leads to more realistic results. Lastly, the modeling results have been validated by comparison with industrial data.

2 Modeling

2.1 Polymerization mechanisms

The modeling approach depends on whether we discuss homopolymerization or copolymerization. In homopolymerization, only one monomer is involved in the production of the polymer, while in copolymerization reaction, there are two types of monomer forming the polymer. In the current study, the kinetic model developed by De Carvalho et al. [23] and McAuley et al. [24] was employed to produce a comprehensive mechanism which describes the kinetics of copolymerization of ethylene and 1-butene catalyzed by two sites of the Z-N catalyst. Table 1 lists the

reactions, comprising formation, initiation, propagation, transfer and deactivation of the active sites. To solve the equations, method of moments was used. These related moments equations are listed in Table 2. The index i in the tables refers to the type of monomer and index j refers to the type of the active site. Table 3 gives the rate constants of each reaction for both site types that were used in this work and mentions their sources in the literature.

If we assume that monomers are primarily consumed over the propagation reactions, we can obtain the equation for consumption rate of each component. Eq. 1 shows this mathematical statement after solving the moment equations [24]:

$$R_k = \sum_j^{ns} \sum_i^{m[} M_k] Y(0,j) k_{p_{ik}} \qquad k = 1,2,.. \tag{1}$$

where m is the number of each type of monomer and ns is the number of each type of active site. Then, we can get the total polymer production from Eq. 2:

$$R_p = \sum_{k=1}^{m} m w_k R_k \tag{2}$$

Table 1

Table 2

Table 3

2.2 Hydrodynamics

2.2.1 Available models

Series and parallel reactions in catalytic polymerization of ethylene with alpha-olefin copolymers makes this process rather complicated. The extensive multi-

site kinetic model proposed by McAuley et al. [24] considers copolymerization of olefins over heterogeneous Z-N catalysts. The main fundamental reactions in polymerization which were considered in this study have been given in Table 1. These reactions include the formation of active centers, insertion of monomers into the growing polymer chains, chain transfer reactions, and catalyst de-activation respectively.

The method of moments is the most frequently used method for modeling polymerization. This is because, by applying this method, we can foretell polymer properties such as density, Polydispersity Index (PDI), average molecular weight, and branching frequency as well as the ability to calculate operating variables, i.e., reactor temperature, rate of polymer production and rate of components consumption (monomers and hydrogen). These moment equations have been given in Table 2.

Kiashemshaki et al. [19] used a semi-dynamic model to predict polymer properties in the sense that they did not produce dynamic temperature and comonomer concentrations profiles in their model . In order to model the gas-phase LLDPE production FBR, they divided the bed into several Plug Flow Reactors (PFR) and CSTRs in series. To model such a reactor, Kiashemshaki et al. [19] made several assumptions, which are as follows:

1. Temperature gradients and radial concentrations in the reactor are negligible.
2. Elutriation of solids from the top of the reactor is neglected.
3. Overall movement direction of polymer particles is assumed to be downwards in both phases.
4. Constant mean particle size is considered through the bed.
5. The heat and mass transfer resistances between the emulsion gas and solid polymer particles are negligible, which is low to moderate catalyst activity.

6. Reaction occurs in both emulsion and bubble phases.
7. Catalyst is fed continuously into the bed as pre-polymer.

2.2.2 Modified dynamic model

In the present work, a modified dynamic two-phase model is developed. Solid entrainment at the top of the reactor has been taken into account since there are cases where elutriation rate cannot be ignored. Normally, most of the granular particles remain in the bed while the smaller ones will leave the reactor with the fluidizing gas. However, where velocities are several times greater than the terminal velocity, coarse particles can also be entrained from the bed [25]. This phenomenon is called particle carry over or particle entrainment, and is very important in the design and operation of FBRs. Elutriation takes place in the cyclone outside the FBR, and the solids are separated from the gas, reentering the reactor after some processing. This shows that in cases were particle entrainment occurs, it is vital to consider their effect on the process. As a result, in the present study, solid entrainment was considered in the model for mass and energy balances to make the results more realistic to the real data. An important property of any polymer grade is its MWD. It has been included in the model in order to check the validation of the model in comparison with industrial data.

In this model, the polymerization reaction is assumed to occur in both emulsion and bubble phases. Equations that are needed to calculate the heat and mass transfer coefficients, velocities in bubble and emulsion phase, and other useful parameters in the two-phase model are listed in Table 4. A concise list of assumptions used in the dynamic two-phase model is as follows:

1. The emulsion phase is considered to be completely mixed and not at the minimum fluidization condition.
2. Polymerization reactions are assumed to take place in both emulsion and bubble phases.
3. The bubbles are considered to be a sphere of constant dimensions and pass with unchanging velocity through the bed at plug flow condition.
4. Resistance of heat and mass transfer among gas and solid in emulsion and bubble phases are neglected.
5. Radial gradients for concentration and temperature in the reactor are neglected as a result of strict mixing brought about by the up-flowing gas.
6. Uniform particle size is considered all over the bed.
7. Solids entrainment is considered at the topmost part of the bed.

Table 4

The mass balances obtained based on the assumptions of this model are as follows:

For Emulsion Phase:

$$[M_i]_{e,(in)}U_eA_e - [M_i]_eU_eA_e - R_v\varepsilon_e[M_i]_e + K_{be}([M_i]_b - [M_i]_e)V_e\left(\frac{\delta}{1-\delta}\right) - (1-\varepsilon_e)R_{i_e} - \frac{K_eV_e\varepsilon_eA_e[M_i]_e}{W_e} = \frac{d}{dt}(V_e\varepsilon_e[M_i]_e) \quad (3)$$

For Bubble Phase:

$$[M_i]_{b,(in)}U_bA_b - [M_i]_bU_bA_b - R_v\varepsilon_b[M_i]_b - \mathrm{K}_{be}([M_i]_b - [M_i]_e)V_b - (1-\varepsilon_b)\frac{A_b}{V_{PFR}}\int Ri_b dz - \frac{K_bV_b\varepsilon_bA_b[M_i]_b}{W_b} = \frac{d}{dt}(V_b\varepsilon_b[M_i]_b) \quad (4)$$

The energy balances are expressed as follows:

For Emulsion Phase:

$$U_e A_e\left(T_{e.(in)} - T_{ref}\right)\sum_{i=1}^{m}[M_i]_{e,(in)}\, C_{pi} - U_e A_e\left(T_e - T_{ref}\right)\sum_{i=1}^{m}[M_i]_e C_{pi} -$$

$$R_v\left(T_e - T_{ref}\right)\left(\sum_{i=1}^{m}\varepsilon_e C_{pi}\,[M_i]_e + (1-\varepsilon_b)\rho_{pol}C_{p.pol}\right) + (1-\varepsilon_e)R_{pe}\Delta H_R -$$

$$H_{be}V_e\left(\frac{\delta}{1-\delta}\right)(T_e - T_b) - V_e\varepsilon_e\left(T_e - T_{ref}\right)\sum_{i=1}^{m} C_{pi}\frac{d}{dt}([M_i]_e) - \frac{K_e A_e}{W_e}\left(T_e -\right.$$

$$\left.T_{ref}\right)\left(\sum_{i=1}^{m}\varepsilon_e C_{pi}\,[M_i]_e + (1-\varepsilon_b)\rho_{pol}C_{p.pol}\right) = \left(V_e\left(\varepsilon_e\sum_{i=1}^{m} C_{pi}[M_i]_e +\right.\right.$$

$$\left.\left.(1-\varepsilon_e)\rho_{pol}C_{p.pol}\right)\right)\frac{d}{dt}\left(T_e - T_{ref}\right) \quad (5)$$

For Bubble Phase:

$$U_b A_b\left(T_{b.(in)} - T_{ref}\right)\sum_{i=1}^{m}[M_i]_{b,(in)}\, C_{pi} - U_b A_b\left(T_b - T_{ref}\right)\sum_{i=1}^{m}[M_i]_b C_{pi} -$$

$$R_v\left(T_b - T_{ref}\right)\left(\sum_{i=1}^{m}\varepsilon_b C_{pi}\,[M_i]_b + (1-\varepsilon_e)\rho_{pol}C_{p.pol}\right) + (1-\varepsilon_b)\frac{A_b\Delta H_R}{V_{PFR}}\int R_{pb}dz +$$

$$H_{be}V_b(T_e - T_b) - V_b\varepsilon_b\left(T_b - T_{ref}\right)\sum_{i=1}^{m} C_{pi}\frac{d}{dt}([M_i]_b) -$$

$$\frac{K_b A_b}{W_b}\left(T_b - T_{ref}\right)\left(\sum_{i=1}^{m}\varepsilon_b C_{pi}\,[M_i]_b + (1-\varepsilon_b)\rho_{pol}C_{p.pol}\right) = \left(V_b\left(\varepsilon_b\sum_{i=1}^{m} C_{pi}[M_i]_b +\right.\right.$$

$$\left.\left.(1-\varepsilon_b)\rho_{pol}C_{p.pol}\right)\right)\frac{d}{dt}\left(T_b - T_{ref}\right) \quad (6)$$

Solid elutriation constants are obtained from Rhodes [25] and are as follows:

$$K_e = 23.7\rho_g U_0\frac{A}{W_e}exp\left(\frac{-5.4U_t}{U_0}\right) \quad (7)$$

$$K_b = 23.7\rho_g U_0\frac{A}{W_b}exp\left(\frac{-5.4U_t}{U_0}\right) \quad (8)$$

$$W_e = AH(1-\varepsilon_e)\rho_{pol} \quad (9)$$

$$W_b = AH(1-\varepsilon_b)\rho_{pol} \quad (10)$$

$$U_t = U_t^*\left[\mu\rho_g^{-2}\left(\rho_{pol} - \rho_g\right)g\right]^{0.33} \quad (11)$$

$$U_t^* = \left[18\left(d_p^*\right)^{-2} + (2.335 - 1.744\emptyset_s)\left(d_p^*\right)^{-0.5}\right]^{-1} \quad (12)$$

for $0.5 < \emptyset_s \leq 1$,

$$d_p^* = d_p\left[\mu^{-2}\rho_g\left(\rho_{pol} - \rho_g\right)g\right]^{0.33} \quad (13)$$

These equations can be solved using the following initial conditions:

$$[M_i]_{b,t=0} = [M_i]_{in} \quad (14)$$

$$T_{b,t=0} = T_{in} \quad (15)$$

$$[M_i]_{e,t=0} = [M_i]_{in} \quad (16)$$

$$T_{e,t=0} = T_{in} \quad (17)$$

These sets of equations have been coded and solved in less than 3 seconds using MATLAB and Simulink.

3 Results and discussion

In order to show how the model responds when tested with real data and to validate it, the operating conditions listed in Table 5 were used in performing the simulation study. The data of four different grades of polyethylene produced at a petrochemical company reported by Kiashemshaki et al. [19] is used to both validate and compare the model. Unless mentioned otherwise, the results are based on the operating conditions for grade BP LL0209 as listed in Table 5.

Table 5

The conditions mentioned in this table are common to produce these grades of polyethylene in industrial reactors. Polymer properties such as molecular weight, PDI and Melt Flow Index (MFI), which are crucial to estimate the quality of a given

polymer, have been calculated based on the kinetic model used in this work. Using methods described by McAuley et al. [24], the weight average and number average molecular weight of polymer can also be calculated.

Polymers are made of many repeated units (monomers) which are chemically attached and make very long chains. Having a perception of polymer chain length is obligatory to comprehend the physical properties of a polymer. Chain length is frequently denoted as the molecular weight of the polymer chain, which is correlated to the number of monomers connected in the chain and the relative molecular mass of the monomers. Nevertheless, all artificial polymers are polydisperse, which means that the length of polymer chains are unequal, and as a result, instead of being a single value, the polymer has a distribution of molecular weights and chain lengths. Consequently, some average molecular weight must be calculated from the molecular weights of all the chains in the polymer sample to define the molecular weight.

Fig. 2 demonstrates how the simulation result, based on the presented model and industrial data of a LLDPE, predicts a narrow MWD for the polymer.

Figure 2: Molecular Weight Distribution of the produced LLDPE

The number average molecular weight is defined as the arithmetic mean of all the molecular weights of the polymer chains in the sample, given by:

$$\bar{M}_n = \frac{\sum N_i M_i}{\sum N_i} \tag{18}$$

where N_i is the number of chains of that molecular weight and M_i is the molecular weight of a chain. $\bar{M}_n$ is measured by approaches that define the number of molecules in a sample of a particular weight and can be predicted by means of polymerization mechanisms. If $\bar{M}_n$ is mentioned for a certain MWD, it means that identical numbers

of molecules are present on both sides of $\bar{M}_n$ in the distribution. On the other hand, the weight average molecular weight is given by:

$$\bar{M}_w = \frac{\sum N_i M_i^2}{\sum N_i M_i} \tag{19}$$

Compared to $\bar{M}_n$, $\bar{M}_w$ takes the molecular weight of a chain into consideration to decide how it contributes to the average molecular weight. The larger the chain gets, the effect of chain on M_w increases. Instead of the number of molecules, weight average molecular weight is defined by procedures which measure the molecular size, such as through light scattering techniques. If $\bar{M}_w$ is mentioned for a certain MWD, it means that identical weight of molecules is present on both sides of M_w in the distribution. These values are illustrated in Fig. 3. This figure shows that it takes less than an hour for the number average and weight average molecular weights of polymer to reach a constant value, since the molecular chain length grows rapidly during this time. As shown in this figure, the ultimate amount of weight average molecular weight reaches almost 99000 kg/mole.

The PDI of a polymer is expressed as the weight average molecular weight to number average molecular weight proportion, and is used as a parameter to tell how broad a polymer MWD and is given by:

$$PDI = \frac{\bar{M}_w}{\bar{M}_n} \tag{20}$$

If a polymer has bigger PDI value, the polymer molecular weight is broader. A polymer with PDI=1 in which all the chain lengths are equivalent (such as a protein) is called a monodisperse polymer. The narrowest artificial polymers built so far which are used for calibration have PDI of 1.02 to 1.10. While chain reactions produce PDI values between 1.5 and 20 while step polymerization reactions usually

PDI values of around 2.0 [26]. The PDI profile throughout the polymerization process is similar to the average molecular weight.

Another important property of a polymer is MFI. It is an analysis method that controls how easily a plastic material flows and is a very important test for quality assurance. In order to measure MFI, the amount of a polymer that flows from a standard instrument over a timed interval is weighed.

The relationship between the molecular weight of polyethylene and its MFI is based on the type proposed by McAuley et al. [24], whose constants have been modified to fit the actual data and is given by the following equation:

$$MFI = 3.346 \times 10^{17} \bar{M}_W^{-3.472} \quad (21)$$

The steady state value of PDI and MFI under the operating conditions given in Table 5 are 4.14 and 0.98 gr/10min respectively. Fig. 3 also shows the evolution of PDI and MFI with time in the reactor.

Figure 3: Evolution of the Melt Flow Index, Polydispersity Index, number and weight average molecular weights over time in the reactor

For model verification purposes, the results of the model presented in this work for PDI and MWD have been compared with the actual plant data and results from the study done by Kiashemshaki et al. [19]. The parity plot of Fig. 4 shows that the current dynamic model has been able to predict the PDI of LLDPE very accurately and very close to the work of Kiashemshaki et al. [19]. As mentioned by the authors, the difference in the calculated PDIs of HDPEs could be due to

considering the same catalyst properties for all the grades. However, catalysts are produced in different batches in this plant and could have slightly different properties and rate constants and hence can result in the deviation from the actual PDIs.

Figure 4: Polydispersity Index comparison of four grades of polyethylene with industrial and literature data

Furthermore, the calculated steady state MWD has been compared with the literature [19] and actual MWD data points for a LLDPE (BP LL0209) and a HDPE (BP HD5218) grade in Fig. 5 for comparison. The actual data have been produced using the GPC data provided by the petrochemical complex. These two figures are produced by calculating and plotting the derivative of cumulative weight fraction against the logarithm of weight average molecular weight, which is a typical GPC output. As can be seen, aside from the slight differences, there is a very good agreement between all sets of data for both cases of LLDPE and HDPE grades.

Although taking solids elutriation into account in the present model leads to predicting the polymer properties such as MFI, PDI and MWD accurately, its main advantages lie in calculating the process parameters such as production rate and reactor temperature more precisely. This is due to the improved dynamic mass and energy balance equations which consider solids entrainment and essentially improves the model to comply more with the real world process data. In addition, this model is able to predict the dynamic behavior of the fluidized bed reactor and can also be used for control study and designing an efficient control system for this highly nonlinear process.

Figure 5: Molecular Weight Distribution comparison of LLDPE and HDPE with industrial and literature data

Polymer production rate during residence time in the FBR is given by Eq. 2 and is shown in Fig. 6. This figure shows the evolution of production rate from the start-up moment when Ziegler-Natta catalyst enters the reactor, and reaction starts until the time that solid particles settle in the FBR, and the fluidized bed moves to the steady state condition and the production rate becomes steady (Fig. 1). This figure also shows polymer production rate in both the bubble and emulsion phases during the polymer residence time in the reactor. The calculated overall production rate soars from almost 7 t/hr in the first hour to almost 10 t/hr in the second hour, and becomes steady at 13.44 t/hr after nearly 5 hours of production. To show the model accuracy and validate the results, the production rate has been plotted against both the industrial data and the model of Kiashemshaki et al. [19]. The horizontal line showing actual data is the amount for the steady state production rate in the industrial FBR. As can be seen, the model was able to accurately predict the steady state production rate and stabilize very close to this data with a deviation of 0.4 tones. The figure also illustrates that nearly 60% of the polymer is produced within the emulsion phase and almost 40% of the total polymer production takes place within the bubble phase. The 20% increase in the production rate in bubble phase in comparison with Kiashemshaki et al. [19] is due to the introduction of recycled elutriated solids into the reactor. This predictably increases the amount of catalysts in the bubble phase and leads to higher production in this phase. Since most of the catalysts are within the emulsion phase, less reaction rate or polymer production in the bubble phase is inevitable.

Figure 6: Evolution of polymer production rate over time in the FBR

The evolution of emulsion phase temperature during the polymer residence time in the reactor is shown in the Fig. 7 for the four different grades of polymer. All grades start from temperatures given in Table 5 and continue to increase with different slopes, and becomes steady after almost 5 hours. For example, it is estimated that the temperature of the LLDPE reaches 78 °C after getting steady around the fifth hour and remains at that temperature. The emulsion phase temperature grows rapidly in less than an hour and reaches 58 °C after one hour from a temperature of 44 °C in the beginning, since the polymerization reaction is exothermic and this graph illustrates this clearly. The final steady state temperatures of this grades are compared with both industrial data and the work of Kiashemshaki et al. [19] in the parity plot of Fig. 8. The lower LLDPE temperature compared with the HDPE temperatures and literature data is due to the higher superficial gas velocity of LLDPE grade compared to HDPE grade. There is a direct relation between superficial gas velocity and the monomer residence time in the reactor, heat removal rate from the reactor, particle mixing and fluidization conditions. In fact, by increasing the superficial gas velocity, gas passes faster through the bed. As a result, more solid particles carry over, the amount of catalysts and polymer particles available in the reactor bed will be reduced, and some monomers may bypass the catalysts, and therefore, reaction extent will be reduced and lead to a reduction in the reaction rate. Less reactions in this exothermic reaction means lower temperatures. Since particle entrainment is considered in this model, this will justify the lower temperature results of this model in LLDPE grade compared to those obtained by Kiashemshaki et al. [19].

Another advantage of the current model is calculating temperatures dynamically. Unlike the presented model in this paper, Kiashemshaki et al.'s [19]

work is not dynamic in terms of calculating both temperature and comonomer concentration. A dynamic model can have the advantage that it can be used as a basis in process control studies to test different approaches to control polymer properties and reactor parameters based on parameters like inlet gas compositions, catalyst input rate, gas superficial velocity, and reactor pressure. Moreover, solids elutriation is another phenomenon in FBRs which cannot be neglected, and is included in this work to make the model be more realistic. Fig. 8 shows that the temperatures calculated in this work are more accurate and closer to actual data.

Figure 7: Evolution of temperature in the emulsion phase for the four different grades of polyethylene

Table 6 shows the operating conditions of another industrial polyethylene production reactor in a second petrochemical complex during one working shift. The operational data and resulting temperature data were collected using plant distributed control system. To further validate the model, it was tested using this dataset. Calculated reactor temperatures have been compared with real data in Fig. 9. The model has again been capable of accurately predicting reactor temperature for this grade of polymer. The average error for this dataset is 0.6 percent deviation from the industrial data, which is small in the engineering context. Nevertheless, considering resistance of heat transfer among gas and solids in both phases, radial temperature gradients in the reactor and particle size distributions could further improve the model, which leads to better prediction of reactor parameters and polymer properties. However, this will increase model complexity and computational efforts.

Figure 8: Emulsion phase temperature comparison with industrial and literature data for the four different grades of polyethylene after reaching steady state

Table 6

Figure 9: Reactor temperature comparison with industrial data during an operating shift

The evolution of mean monomer concentrations throughout the bed during the residence time in the reactor are shown in Fig. 10. It is clear that the time of getting into a steady state is the same as production rate and temperature profile graphs. As can be seen, ethylene as monomer and 1-butene as comonomer are consumed through the copolymerization reaction in order to produce the polymer. As a result, their concentrations decrease exponentially during the first 5 hours of the residence time before going flat in the steady zone.

Figure 10: Evolution of mean ethylene and 1-butene concentration throughout the bed during residence time in the FBR

Another imperative property of the polymer is its density. Several polymer grades for different applications need to have specific densities. Since this model is dynamic, it is capable to be used in future polymer density control studies. However, it is very complicated to find the correlation between density and polymer structure. Density could be altered by both the length and number of the short chain branches and to a small extent by the polymer molecular weight [27]. McAuley et al. [24] developed an experimental equation to relate the amount of comonomer in linear polyethylene to its density:

$$\rho = 0.966 - \alpha C_x^{\beta} \quad (22)$$

Where α and β are parameters which depend on comonomer, and C_x is the comonomer mole percent in the polymer. α and β have been fitted at 0.02386 and 0.514 for butane grade polymers. Fig. 11 shows the correlation between 1-butene concentration of the feed and the density calculated from Eq. 22. Naturally, increasing 1-butene concentration leads to lower density values and it can be used as a

manipulated variable in future process control studies to regulate the polymer density value.

Figure 11: Relation between 1-butene concentration of the feed and polymer density

4 Conclusion

A comprehensive two-phase model was developed to predict industrial scale gas-phase ethylene copolymerization reactors. The model considers solid entrainment in the FBR modelling. The hydrodynamic model coupled with a kinetic copolymerization model (ethylene and 1-butene) provides a more detailed understanding of the system.

The model was capable of predicting vital reactor parameters like rate of polymer production and polymer temperature. Moreover, the kinetic model was capable of predicting polymer properties such as PDI, average molecular weights and MWD of the polymer. The PDI, MWD, production rate and reactor temperature results of this model were compared with actual plant data and literature to show the data agreement. This model provides a tool to study the operational, hydrodynamics and kinetic parameters on reactor performance in addition to polymer properties, and can be used as a base for control studies to regulate properties like PDI, MFI or density of a polymer in future works.

Acknowledgement

The authors would like to thank the support of the Research Council of University of Malaya under High Impact Research Grant (UM.C/625/1/HIR/MOHE/ENG/25) and Postgraduate Research Grant (PPP) project No. PG131-2014A.

Nomenclature

A	cross sectional area of the reactor (m^2)
$[M_i]$	concentration of component *i* in the reactor ($kmol/m^3$)
$[M_i]_{in}$	concentration of component *i* in the inlet gaseous stream
$AlEt_3$	triethyl aluminum co-catalyst
Ar	Archimedes number
B_i	moles of reacted monomer bound in the polymer in the reactor
CFD	computational fluid dynamics
$C_{p,pol}$	specific heat capacity of solid product (J/kg.K)
C_{pg}	specific heat capacity of gaseous stream (J/kg.K)
C_{pi}	specific heat capacity of component i (J/kg.K)
C_{pMi}	specific heat capacity of the component i (J/kg.K)
d_b	bubble diameter (m)
d_{b0}	initiate bubble diameter (m)
D_g	gas diffusion coefficient (m^2/s)
d_p	particle diameter (m)
D_t	reactor diameter (m)
FBR	fluidized-bed reactor
F_{cat}	catalyst feed rate (kg/s)
fi	fraction of total monomer in the reactant gas which is monomer M_i
g	gravitational acceleration (m/s2)
GPC	gel permeation chromatography
H	height of the reactor (m)
H_2	hydrogen
H_{bc}	bubble to cloud heat transfer coefficient ($W/m^3.K$)
H_{be}	bubble to emulsion heat transfer coefficient ($W/m^3.K$)
H_{ce}	cloud to emulsion heat transfer coefficient ($W/m^3.K$)
$HDPE$	high-density polyethylene
i	monomer type
I_m	impurity such as carbon monoxide ($kmol/m^3$)
J	active site type
K_b	elutriation constant in bubble phase ($kg\ m^2\ s^{-1}$)
K_{bc}	bubble to cloud mass transfer coefficient (s^{-1})
K_{be}	bubble to emulsion mass transfer coefficient (s^{-1})
K_{ce}	cloud to emulsion mass transfer coefficient (s^{-1})
$k_{dI}(j)$	deactivation by impurities rate constant for a site of type *j*
$k_{ds}(j)$	spontaneous deactivation rate constant for a site of type *j*
K_e	elutriation constant in emulsion phase ($kg\ m^2\ s^{-1}$)
$k_f(j)$	formation rate constant for a site of type *j*
$k_{fhi}(j)$	transfer rate constant for a site of type *j* with terminal monomer M_i reacting with hydrogen
$k_{fmi}(j)$	transfer rate constant for a site of type *j* with terminal monomer M_i reacting with monomer M_k
$k_{fri}(j)$	transfer rate constant for a site of type *j* with terminal monomer M_i reacting with $AlEt_3$
$k_{fsi}(j)$	spontaneous transfer rate constant for a site of type *j* with terminal monomer M_i
k_g	gas thermal conductivity (W/m.K)
$k_{hi}(j)$	rate constant for reinitiating of a site of type *j* by monomer M_i
$k_{hr}(j)$	rate constant for reinitiating of a site of type *j* by cocatalyst

$ki_i\ (j)$	rate constant for initiation of a site of type *j* by monomer M_i
$kp_{ik}\ (j)$	propagation rate constant for a site of type *j* with terminal monomer M_i reacting with monomer M_k
kp_{Ti}	propagation rate constant (m3/kmol s)
LLDPE	linear low-density polyethylene
MFI	melt flow index (g/10 min)
Mn	number average molecular weight of polymer *(kg/kmol)*
Mw	weight average molecular weight of polymer *(kg/kmol)*
MWD	molecular weight distribution
mw_i	molecular weight of monomer i (g/mol)
$N\ (0, j)$	uninitiated site of type j produced by formation reaction
$N^*(j)$	potential active site of type j
$N_d\ (j)$	spontaneously deactivated site of type j
$N_{dIH}\ (0, j)$	impurity killed sites of type j
N_H	uninitiated site of type j produced by transfer to hydrogen reaction
$N_j\ (r, j)$	living polymer molecule of length r, growing at an active site of type j, with terminal monomer M
P	pressure (Pa)
PDI	polydispersity index
$Q\ (r, j)$	dead polymer molecule of length r produced at a site of type j
r	number of units in polymer chain
Re_{mf}	Reynolds number of particles at minimum fluidization condition
R_i	instantaneous consumption rate of monomer (kmol/s)
R_p	production rate (kg/s)
R_v	volumetric polymer outflow from the reactor (m^3/s)
T	temperature (K)
t	time (s)
T_{in}	temperature of the inlet gaseous stream (K)
Tref	reference temperature (K)
U_t^*	dimensionless terminal falling velocity coefficient
U_0	superficial gas velocity (m/s)
U_b	bubble velocity (m/s)
U_{br}	bubble rise velocity (m/s)
U_{mf}	minimum fluidization velocity (m/s)
U_t	terminal velocity of falling particles (m/s)
V	reactor volume (m^3)
V_p	volume of polymer phase in the reactor (m^3)
W_b	weight of solids in the bubble phase (kg)
W_e	weight of solids in the emulsion phase (kg)
$X\ (n, j)$	nth moment of chain length distribution for dead polymer produced at a site of type j
$Y(n,j)$	*n*th moment of chain length distribution for living polymer produced at a site of type *j*
Z-N	*Ziegler-Natta catalyst*

Greek letters

ΔH_R	heat of reaction (J/kg)
δ	volume fraction of bubbles in the bed
ε_b	void fraction of bubble for Geldart B particles
ε_e	void fraction of emulsion for Geldart B particles
ε_{mf}	void fraction of the bed at minimum fluidization

μ	gas viscosity (Pa s)
ρ_g	gas density (kg/m^3)
ρ_{pol}	polymer density (kg/m^3)
ϕ_s	sphericity for sphere particles

Subscripts and superscripts

1	ethylene
2	1-butene
b	bubble phase
e	emulsion phase
i	component type number
j	active site type number
mf	minimum fluidization
pol	polymer
ref	reference condition
T,TT	Pseudo kinetic rate constants

References

[1] P. Cai, L. Chen, J. van Egmond, M. Tilston, Some recent advances in fluidized-bed polymerization technology, Particuology. 8 (2010) 578–581.

[2] M. Alizadeh, N. Mostoufi, S. Pourmahdian, R. Sotudeh-Gharebagh, Modeling of fluidized bed reactor of ethylene polymerization, Chem. Eng. J. 97 (2004) 27–35.

[3] T. Xie, K.B. McAuley, J.C.C. Hsu, D.W. Bacon, Gas Phase Ethylene Polymerization: Production Processes, Polymer Properties, and Reactor Modeling, Ind. Eng. Chem. Res. 33 (1994) 449–479. doi:10.1021/ie00027a001.

[4] K.-Y. Choi, W. Harmon Ray, The dynamic behaviour of fluidized bed reactors for solid catalysed gas phase olefin polymerization, Chem. Eng. Sci. 40 (1985) 2261–2279. doi:10.1016/0009-2509(85)85128-9.

[5] F.A.N. Fernandes, L.M. Ferrareso Lona, Fluidized-bed reactor modeling for polyethylene production, J. Appl. Polym. Sci. 81 (2001) 321–332. doi:10.1002/app.1442.

[6] K.B. McAuley, J.P. Talbot, T.J. Harris, A comparison of two-phase and well-mixed models for fluidized-bed polyethylene reactors, Chem. Eng. Sci. 49 (1994) 2035–2045.

[7] R. Jafari, R. Sotudeh-Gharebagh, N. Mostoufi, Performance of the wide-ranging models for fluidized bed reactors, Adv. Powder Technol. 15 (2004) 533–548. doi:10.1163/1568552042000192.

[8] H.T. Bi, J. Li, Multiscale analysis and modeling of multiphase chemical reactors, Adv. Powder Technol. 15 (2004) 607–627. doi:10.1163/1568552042456223.

[9] F. Fernandes, L. Lona, Heterogeneous modeling for fluidized-bed polymerization reactor, Chem. Eng. Sci. 56 (2001) 963–969. doi:10.1016/S0009-2509(00)00311-0.

[10] H. Hatzantonis, H. Yiannoulakis, A. Yiagopoulos, C. Kiparissides, Recent developments in modeling gas-phase catalyzed olefin polymerization fluidized-bed reactors: The effect of bubble size variation on the reactor's performance, Chem. Eng. Sci. 55 (2000) 3237–3259.

[11] Z.-W. Zheng, D.-P. Shi, P.-L. Su, Z.-H. Luo, X.-J. Li, Steady-State and Dynamic Modeling of the Basell Multireactor Olefin Polymerization Process, Ind. Eng. Chem. Res. 50 (2011) 322–331. doi:10.1021/ie101699b.

[12] Z.-H. Luo, P.-L. Su, D.-P. Shi, Z.-W. Zheng, Steady-state and dynamic modeling of commercial bulk polypropylene process of Hypol technology, Chem. Eng. J. 149 (2009) 370–382. doi:http://dx.doi.org/10.1016/j.cej.2009.01.021.

[13] O. Ashrafi, H. Nazari-pouya, N. Mostoufi, Particle Size Distribution in Gas-phase Polyethylene Reactors, Adv. Powder Technol. 19 (2008) 321–334.

[14] D.Y. Khang, H.H. Lee, Particle size distribution in fluidized beds for catalytic polymerization, Chem. Eng. Sci. 52 (1997) 421–431. doi:10.1016/S0009-2509(97)86701-2.

[15] C.D. Immanuel, C.F. Cordeiro, S.S. Sundaram, E.S. Meadows, T.J. Crowley, F.J. Doyle, Modeling of particle size distribution in emulsion co-polymerization: comparison with experimental data and parametric sensitivity studies, Comput. Chem. Eng. 26 (2002) 1133–1152. doi:10.1016/S0098-1354(02)00031-5.

[16] M.R. Tamadondar, H. Azizpour, R. Zarghami, N. Mostoufi, J. Chaouki, Using particle trajectory for determining the fluidization regime in gas–solid fluidized beds, Adv. Powder Technol. 23 (2012) 349–351. doi:10.1016/j.apt.2011.04.012.

[17] Y.. Makkawi, P.. Wright, Fluidization regimes in a conventional fluidized bed characterized by means of electrical capacitance tomography, Chem. Eng. Sci. 57 (2002) 2411–2437. doi:10.1016/S0009-2509(02)00138-0.

[18] A.J. Sederman, L.F. Gladden, M.D. Mantle, Application of magnetic resonance imaging techniques to particulate systems, Adv. Powder Technol. 18 (2007) 23–38. doi:10.1163/156855207779768232.

[19] A. Kiashemshaki, N. Mostoufi, R. Sotudeh-Gharebagh, Two-phase modeling of a gas phase polyethylene fluidized bed reactor, Chem. Eng. Sci. 61 (2006) 3997–4006.

[20] A. Shamiri, M.A. Hussain, F. sabri Mjalli, N. Mostoufi, S. Hajimolana, Dynamics and Predictive Control of Gas Phase Propylene Polymerization in Fluidized Bed Reactors, Chinese J. Chem. Eng. 21 (2013) 1015–1029. doi:http://dx.doi.org/10.1016/S1004-9541(13)60565-0.

[21] A. Shamiri, S. Wei, M. Fauzi, M.A. Hussain, N. Mostoufi, Modified two-phase model with hybrid control for gas phase propylene copolymerization in fluidized bed reactors, Chem. Eng. J. 264 (2015) 706–719. doi:10.1016/j.cej.2014.11.104.

[22] A. Shamiri, M.A. Hussain, F.S. Mjalli, N. Mostoufi, Improved single phase modeling of propylene polymerization in a fluidized bed reactor, Comput. Chem. Eng. 36 (2012) 35–47.

[23] A.B. de Carvalho, P.E. Gloor, A.E. Hamielec, A kinetic mathematical model for heterogeneous Ziegler-Natta copolymerization, Polymer (Guildf). 30 (1989) 280–296. doi:10.1016/0032-3861(89)90118-3.

[24] K.B. McAuley, J.F. MacGregor, A.E. Hamielec, A kinetic model for industrial gas-phase ethylene copolymerization, AIChE J. 36 (1990) 837–850. doi:10.1002/aic.690360605.

[25] M. Rhodes, Introduction to Particle Technology, John Wiley & Sons Ltd, 2008.

[26] D. Braun, H. Cherdron, H. Ritter, Polymer Synthesis: Theory and Practice: Fundamentals, Methods, Experiments, Springer Science & Business Media, 2013.

[27] K.B. Sinclair, Characteristic of linear LPPE and description of UCC gas phase process, Process Econ. Report, SRI Int. Menlo Park. CA. (1983).

List of figures

List of tables

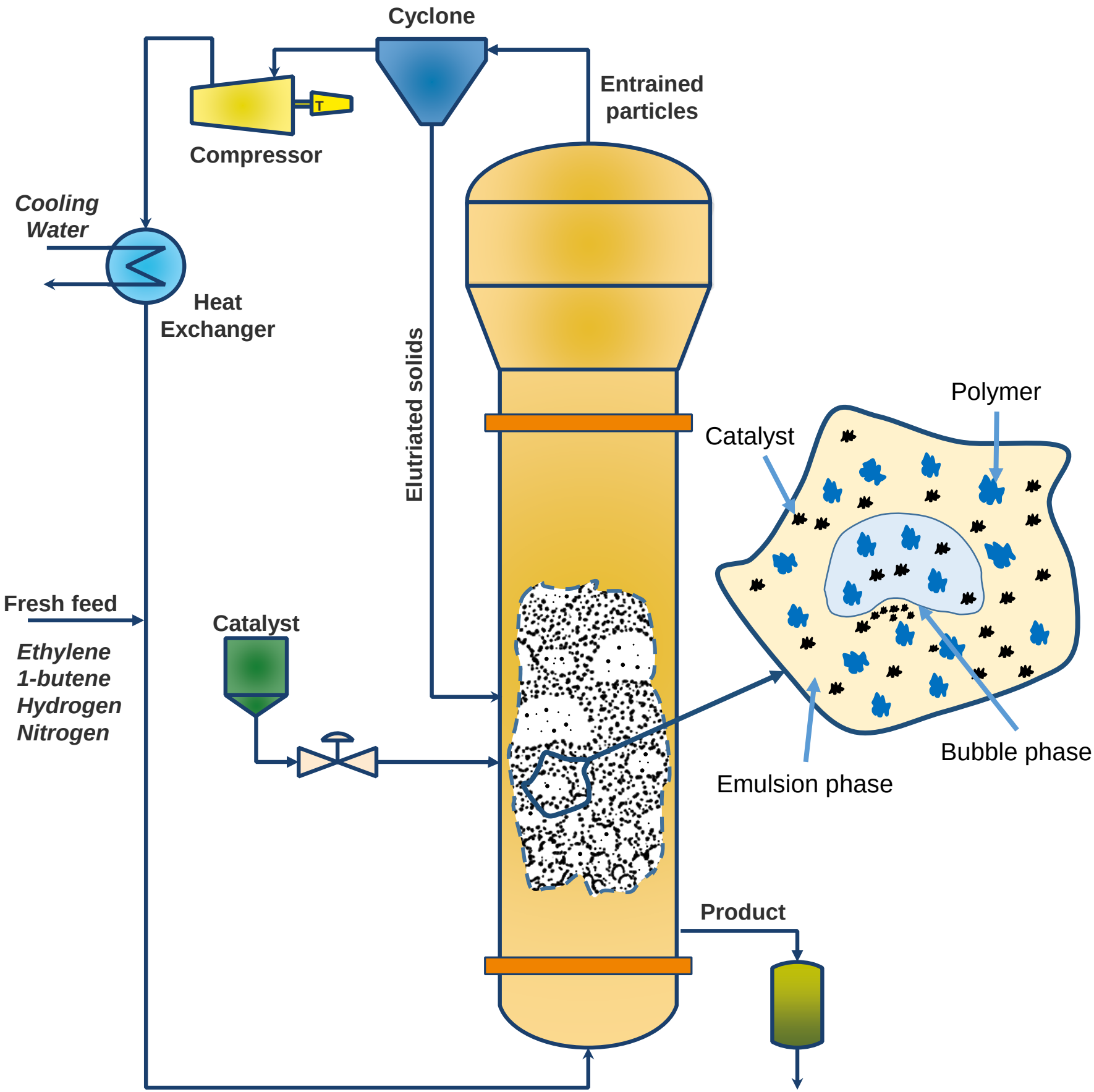
Cyclone
Entrained particles
Compressor
T
Cooling Water
Heat Exchanger
Elutriated solids
Polymer
Catalyst
Fresh feed
Ethylene
1-butene
Hydrogen
Nitrogen
Catalyst
Bubble phase
Emulsion phase
Product

Figure 2

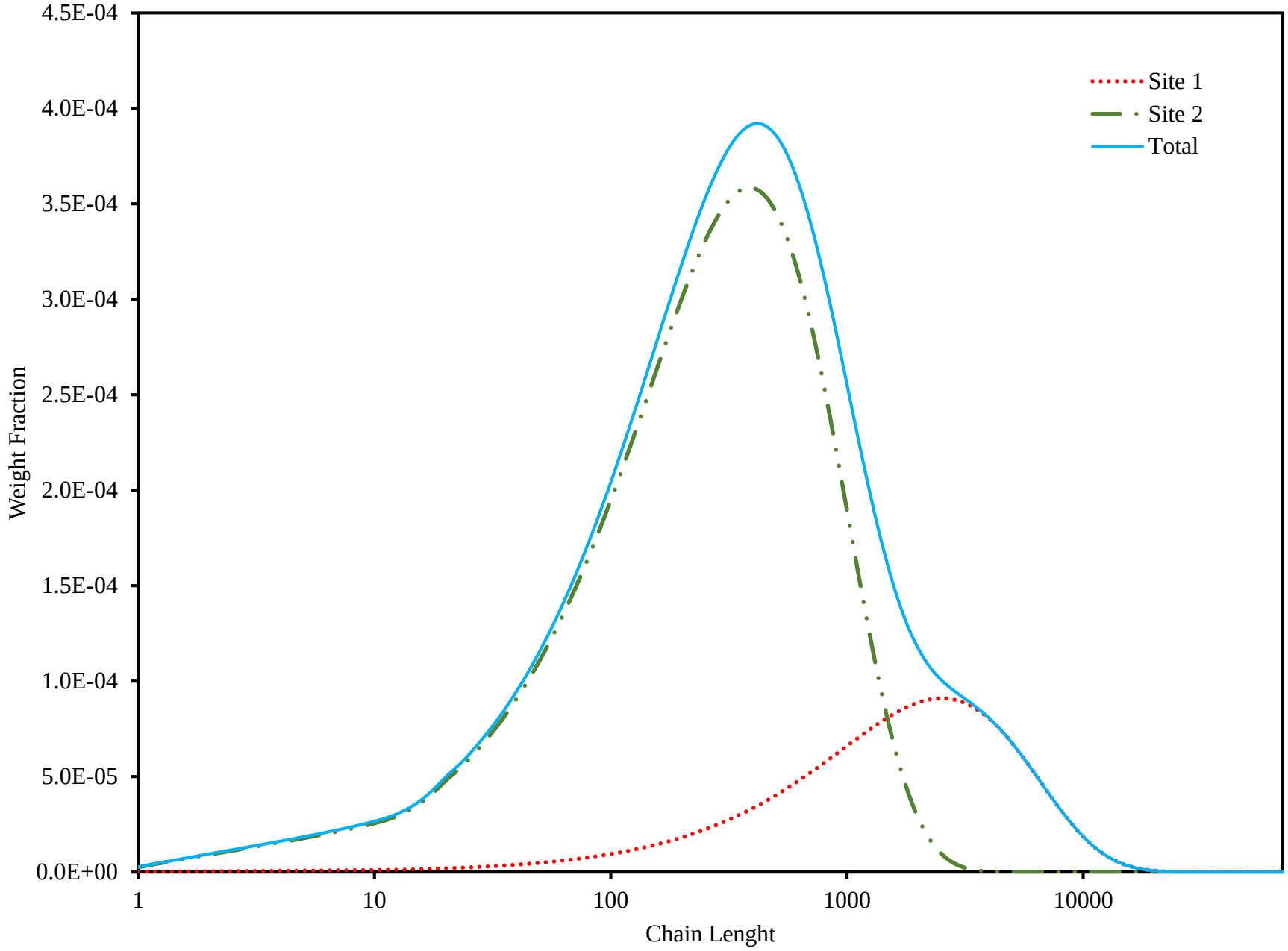
4.5E-04
4.0E-04
3.5E-04
3.0E-04
2.5E-04
2.0E-04
1.5E-04
1.0E-04
5.0E-05
0.0E+00
Weight Fraction
1
10
100
1000
10000
Chain Lenght
Site 1
Site 2
Total

Figure 3

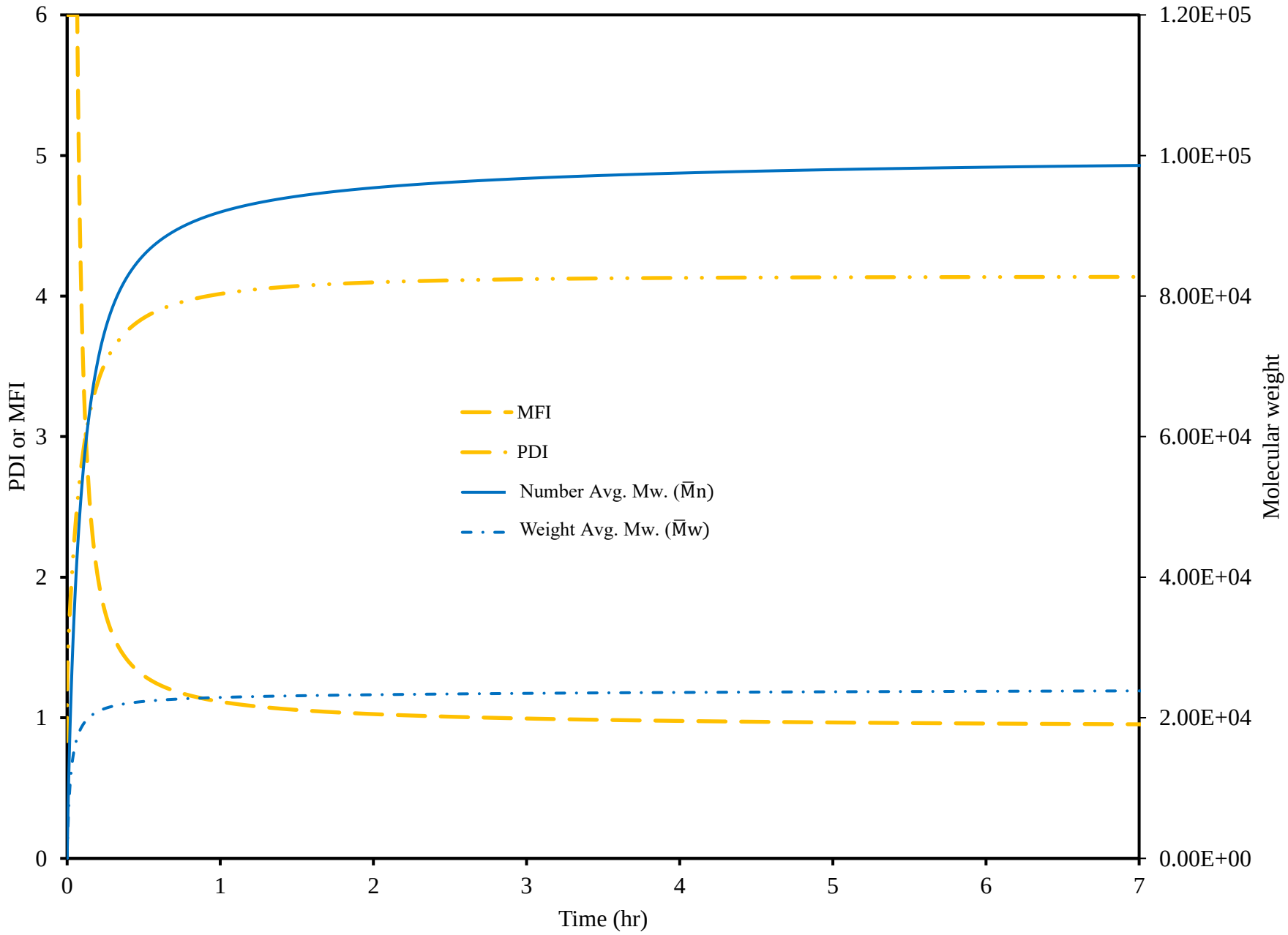
6
5
4
3
2
1
0
PDI or MFI
1.20E+05
1.00E+05
8.00E+04
6.00E+04
4.00E+04
2.00E+04
0.00E+00
Molecular weight
0
1
2
3
4
5
6
7
Time (hr)
MFI
PDI
Number Avg. Mw. (M̄n)
Weight Avg. Mw. (M̄w)

Figure 4

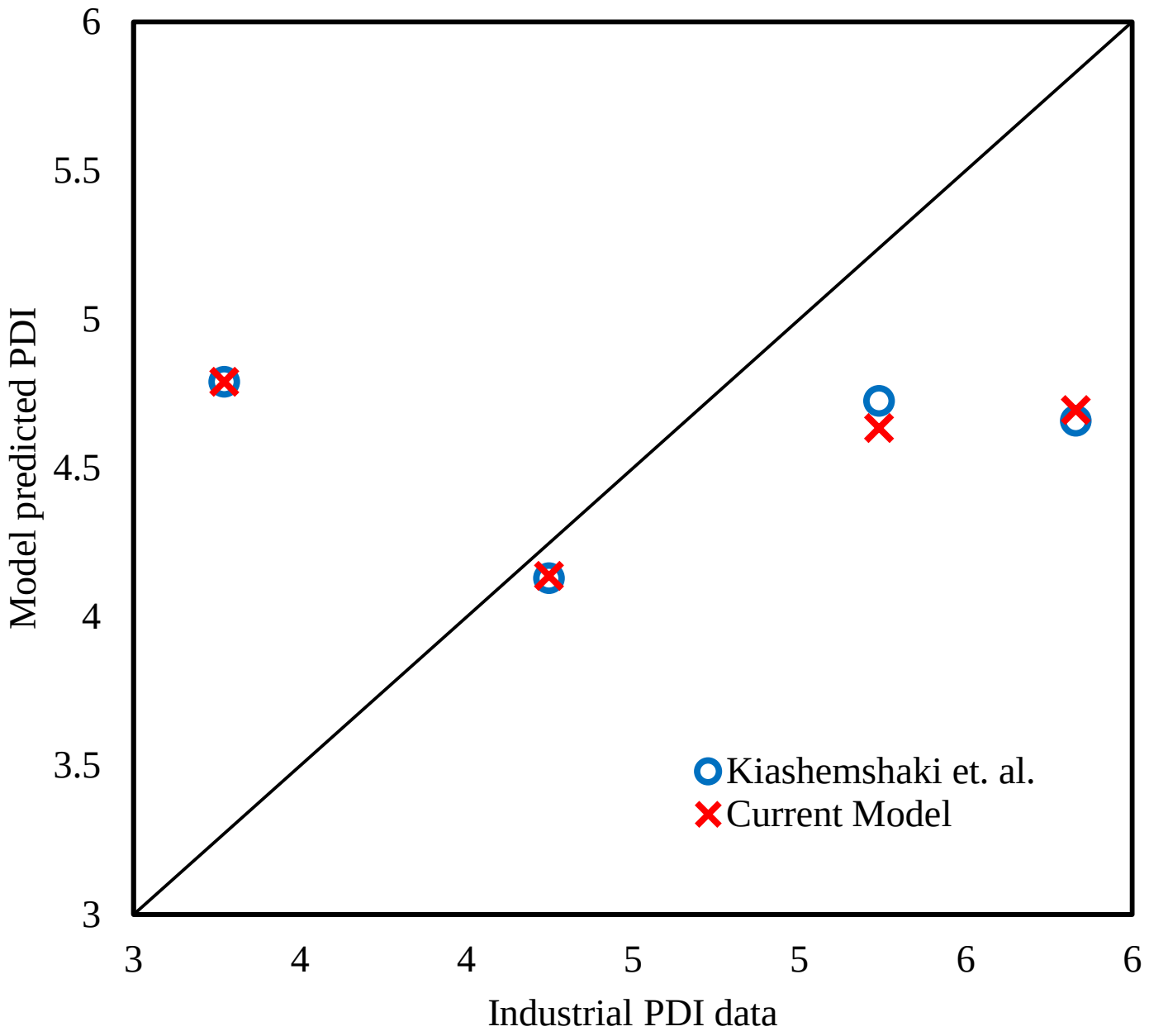
Model predicted PDI
Industrial PDI data
6
5.5
5
4.5
4
3.5
3
3
4
4
5
5
6
6
Kiashemshaki et. al.
Current Model

Figure 5

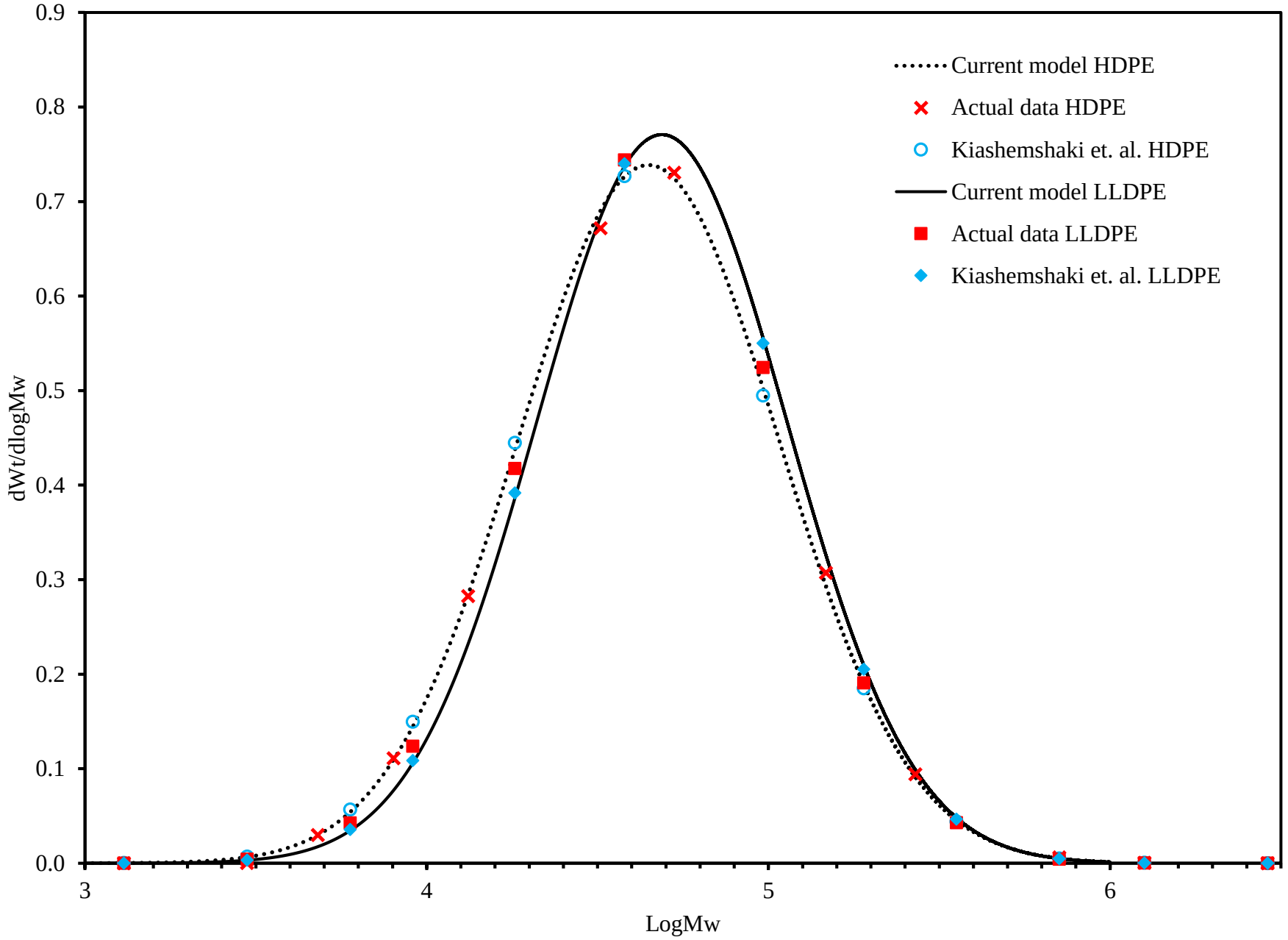
0.9
0.8
0.7
0.6
0.5
0.4
0.3
0.2
0.1
0.0
dWt/dlogMw
3
4
5
6
LogMw
Current model HDPE
Actual data HDPE
Kiashemshaki et. al. HDPE
Current model LLDPE
Actual data LLDPE
Kiashemshaki et. al. LLDPE

Figure 6

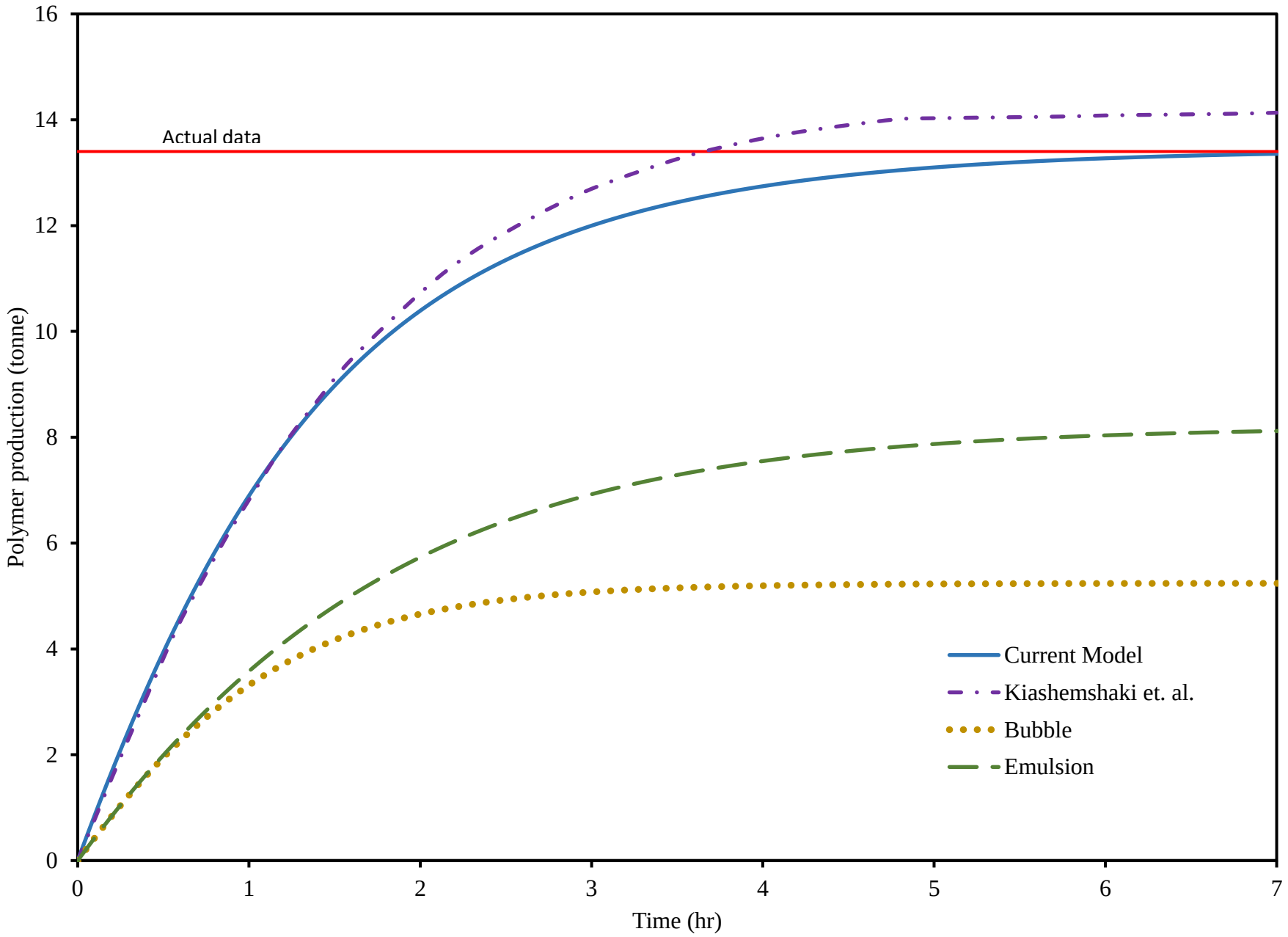
16
14
12
10
8
6
4
2
0
Actual data
Polymer production (tonne)
0
1
2
3
4
5
6
7
Time (hr)
Current Model
Kiashemshaki et. al.
Bubble
Emulsion

Figure 7

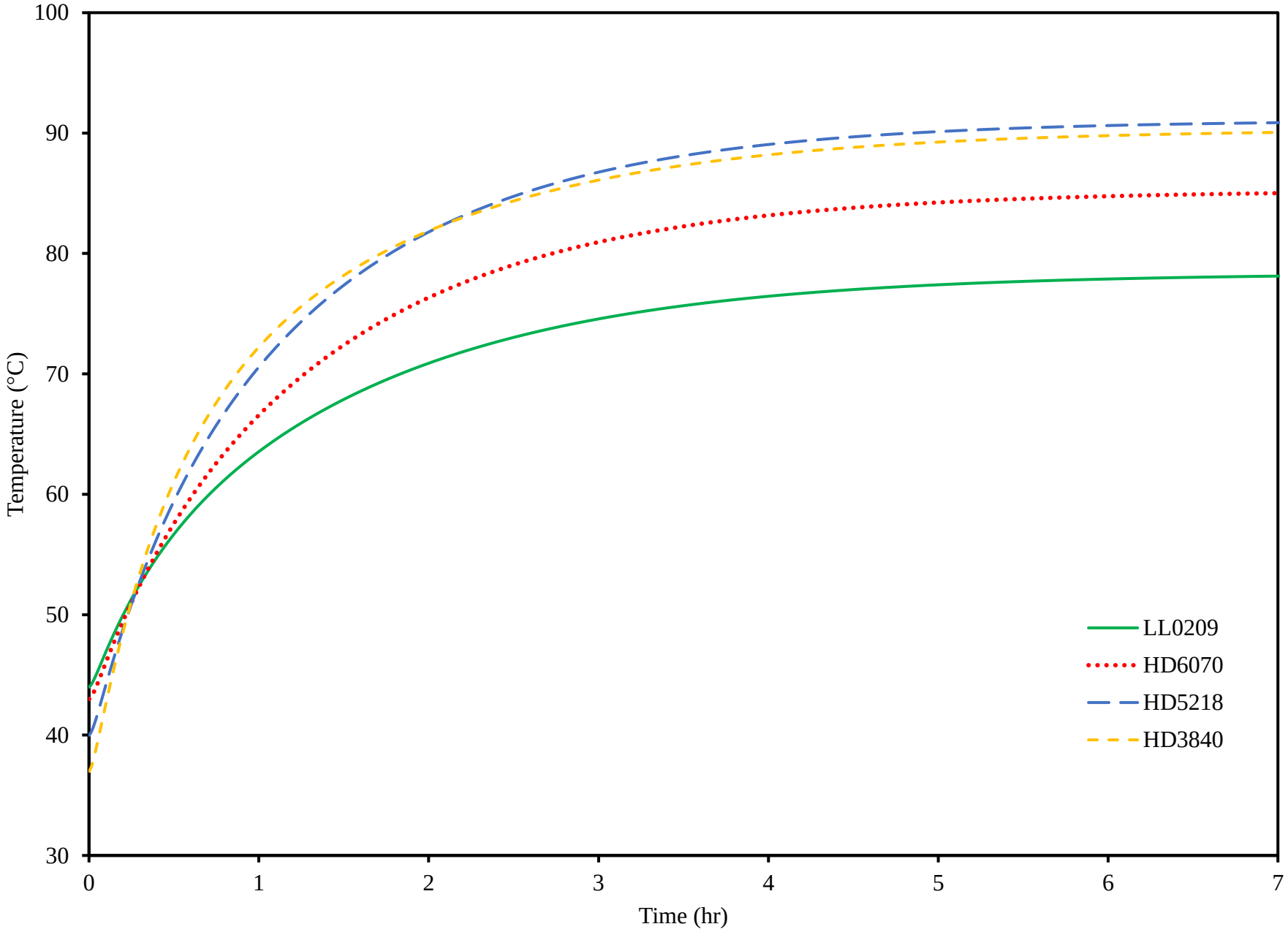
100
90
80
70
60
50
40
30
Temperature (°C)
0
1
2
3
4
5
6
7
Time (hr)
LL0209
HD6070
HD5218
HD3840

Figure 8

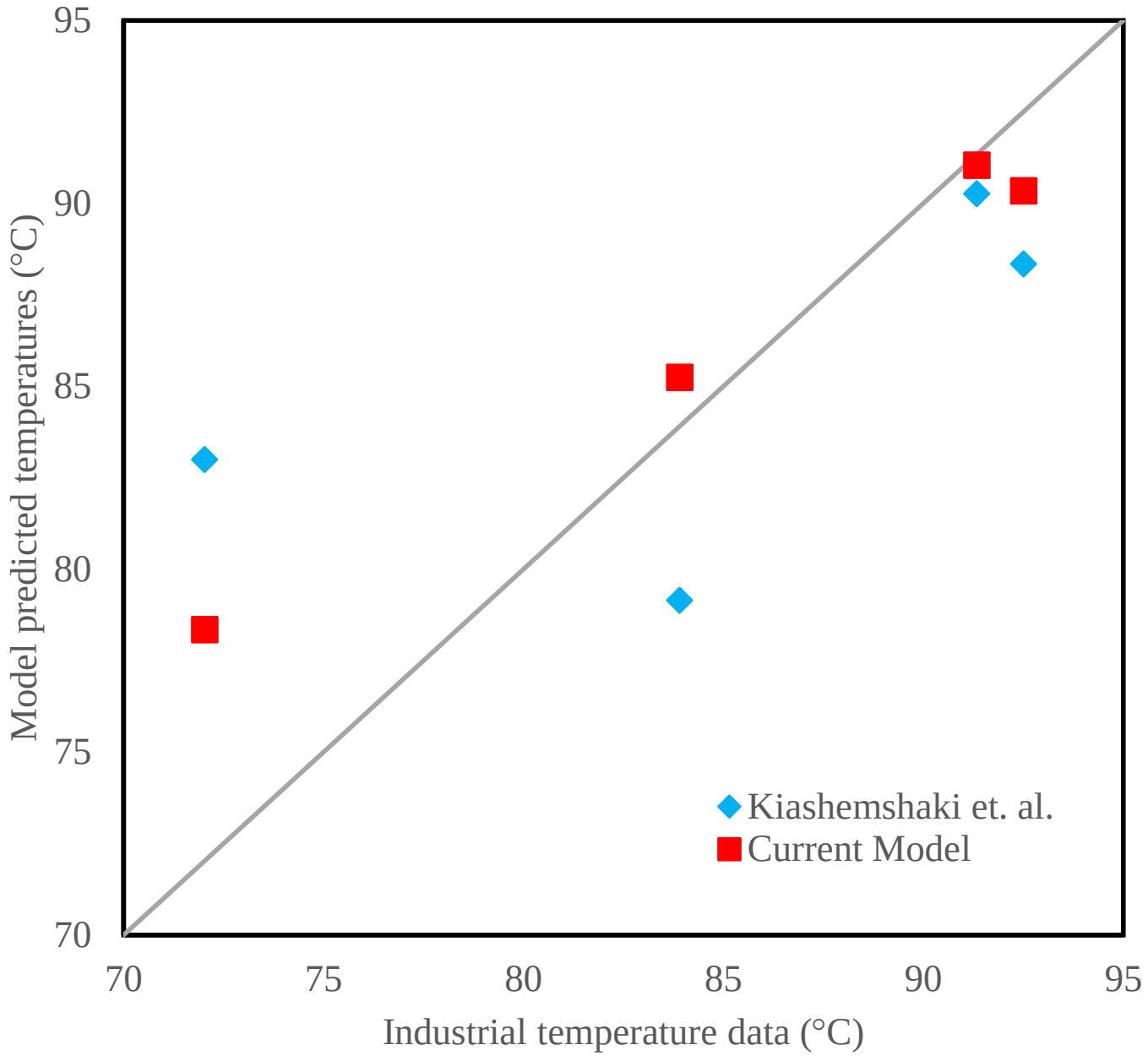
95
90
85
80
75
70
Model predicted temperatures (°C)
70
75
80
85
90
95
Industrial temperature data (°C)
Kiashemshaki et. al.
Current Model

Figure 9

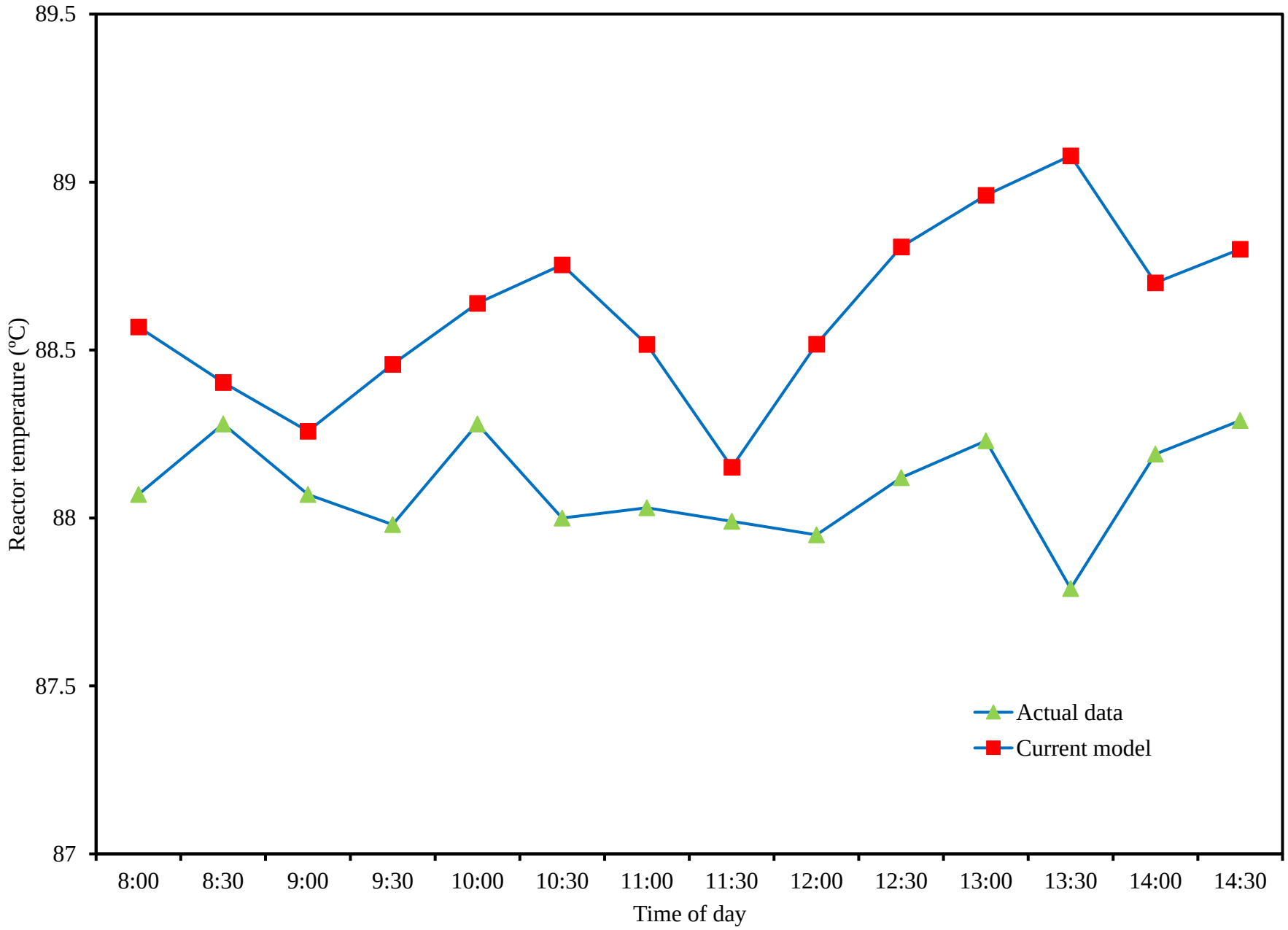
89.5
89
88.5
88
87.5
87
Reactor temperature (°C)
8:00
8:30
9:00
9:30
10:00
10:30
11:00
11:30
12:00
12:30
13:00
13:30
14:00
14:30
Time of day
Actual data
Current model

Figure 10

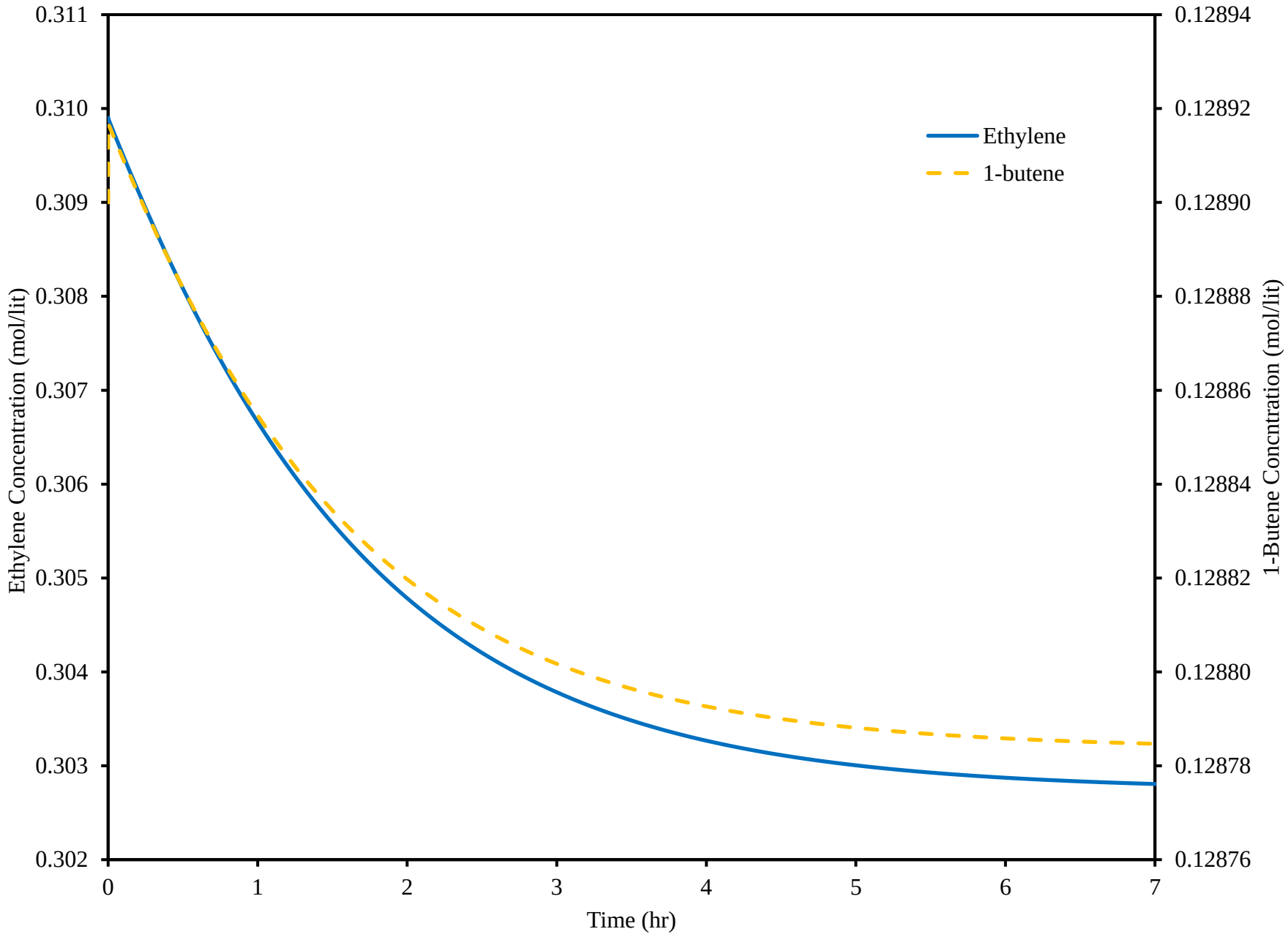
0.311
0.310
0.309
0.308
0.307
0.306
0.305
0.304
0.303
0.302
Ethylene Concentration (mol/lit)
0.12894
0.12892
0.12890
0.12888
0.12886
0.12884
0.12882
0.12880
0.12878
0.12876
1-Butene Concntration (mol/lit)
0
1
2
3
4
5
6
7
Time (hr)
Ethylene
1-butene

Figure 11

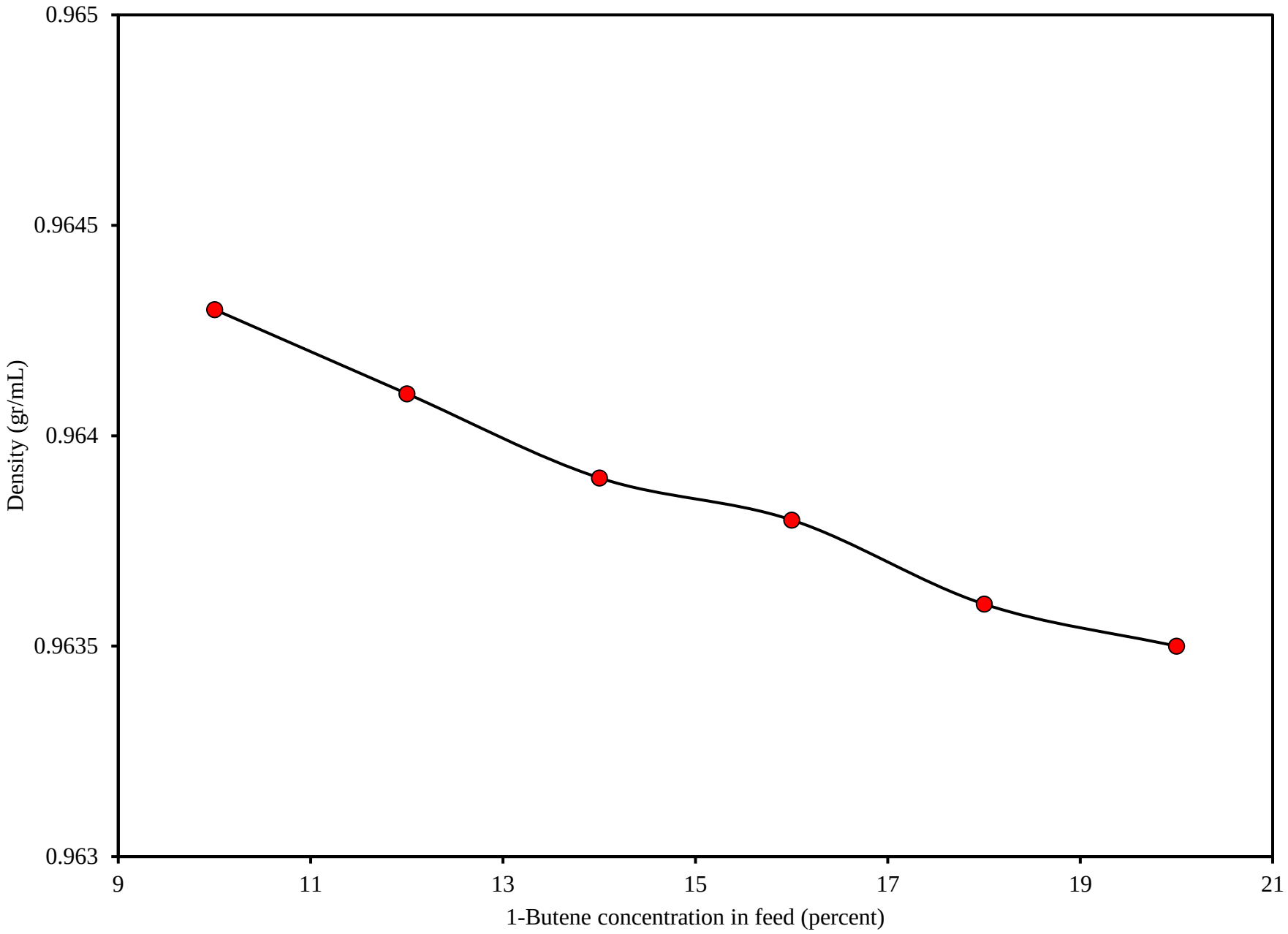
0.965
0.9645
0.964
0.9635
0.963
Density (gr/mL)
9
11
13
15
17
19
21
1-Butene concentration in feed (percent)

Table 1

Table 1: Reactions occurring in a copolymerization reaction [24]

Description	Reaction
Formation reaction	$N^{*}(j) \xrightarrow{kf(j)} N(0,j)$
Initiation reaction	$N(0,j) + M_i \xrightarrow{ki_i(j)} N_i(1,j) \quad i = 1,2,..$
Propagation	$N_i(r,j) + M_k \xrightarrow{kp_{ik}(j)} N_k(r+1,j) \quad i = k = 1,2,..$
Transfer to monomer	$N_i(r,j) + M_k \xrightarrow{kfm_{ik}(j)} N_k(1,j) + Q(r,j) \quad i = k = 1,2,..$
Transfer to hydrogen	$N_i(r,j) + H_2 \xrightarrow{kfh_i(j)} N_H(0,j) + Q(r,j) \quad i = 1,2,..$
	$N_H(0,j) + M_i \xrightarrow{kh_i(j)} N_i(1,j) \quad i = 1,2,..$
	$N_H(0,j) + AlEt_3 \xrightarrow{kh_r(j)} N_1(1,j)$
Transfer to co-catalyst	$N_i(r,j) + AlEt_3 \xrightarrow{kfr_i(j)} N_1(1,j) + Q(r,j) \quad i = 1,2,..$
Spontaneous transfer	$N_i(r,j) \xrightarrow{kfs_i(j)} N_H(0,j) + Q(r,j) \quad i = 1,2,..$
Deactivation reactions	$N_i(r,j) \xrightarrow{kds_i(j)} N_d(j) + Q(r,j) \quad i = 1,2,..$
	$N(0,j) \xrightarrow{kds(j)} N_d(j)$
	$N_H(0,j) \xrightarrow{kds(j)} N_d(j)$
Reactions with poisons	$N_i(r,j) + I_m \xrightarrow{kdI(j)} N_{dIH}(0,j) + Q(r,j) \quad i = 1,2,..$
	$N_H(0,j) + I_m \xrightarrow{kdI(j)} N_{dIH}(0,j)$
	$N(0,j) + I_m \xrightarrow{kdI(j)} N_{dI}(0,j)$

Table 2

Table 2: Moments equations resulted from Table 1

$\frac{dY(0,j)}{dt} = [M_T]\{k_{i_T}(j)N(0,j) + k_{h_T}(j)N_H(0,j)\} + k_{h_r}(j)N_H(0,j)[AlEt_3] - Y(0,j)\left\{k_{fh_T}(j)[H_2] + k_{fs_T}(j) + k_{ds}(j) + k_{dI}(j)[I_m] + \frac{R_v}{V_p}\right\}$
$\frac{dY(1,j)}{dt} = [M_T]\{k_{i_T}(j)N(0,j) + k_{h_T}(j)N_H(0,j)\} + k_{h_r}(j)N_H(0,j)[AlEt_3] + [M_T]k_{p_{TT}}(j)Y(0,j) + \{Y(0,j) - Y(1,j)\}\{k_{fm_{TT}}(j)[M_T] + k_{fr_T}(j)[AlEt_3]\}$ $- Y(1,j)\left\{k_{fh_T}(j)[H_2] + k_{fs_T}(j) + k_{ds}(j) + k_{dI}(j)[I_m] + \frac{R_v}{V_p}\right\}$
$\frac{dY(2,j)}{dt} = [M_T]\{k_{i_T}(j)N(0,j) + k_{h_T}(j)N_H(0,j)\} + k_{h_r}(j)N_H(0,j)[AlEt_3] + \{[M_T]k_{p_{TT}}(j)2Y(1,j) - Y(0,j)\}$ $+ \{Y(0,j) - Y(2,j)\}\{k_{fm_{TT}}(j)[M_T] + k_{fr_T}(j)[AlEt_3]\} - Y(2,j)\left\{k_{fh_T}(j)[H_2] + k_{fs_T}(j) + k_{ds}(j) + k_{dI}(j)[I_m] + \frac{R_v}{V_p}\right\}$
$\frac{dX(n,j)}{dt} = \{Y(n,j) - N_T(1,j)\}\{k_{fm_{TT}}(j)[M_T] + k_{fr_T}(j)[AlEt_3] + k_{fh_T}(j)[H_2] + k_{fs_T}(j) + k_{ds}(j) + k_{dI}(j)[I_m]\} - X(n,j)\frac{R_v}{V_p} \quad n = 0,1,2$

Note: Rate constants with subscript $_T$ and $_{TT}$ are pseudo-kinetic rate constants. The full description and calculation method is given by McAuley et. al. [24]

Table 3

Table 3: Reaction rate constants for polyethylene copolymerization [24]

Reaction	Rate constant	Unit	Site type 1	Site type 2
Formation	$k_f(j)$	s^{-1}	1	1
Initiation	$k_{i_1}(j)$	L/kmol s	1	1
	$k_{i_2}(j)$	L/kmol s	0.14	0.14
	$k_{h_1}(j)$	L/kmol s	1	1
	$k_{h_2}(j)$	L/kmol s	0.1	0.1
	$k_{h_r}(j)$	L/kmol s	20	20
Propagation	$k_{p_{11}}(j)$	L/kmol s	85	85
	$k_{p_{12}}(j)$	L/kmol s	2	15
	$k_{p_{21}}(j)$	L/kmol s	64	64
	$k_{p_{22}}(j)$	L/kmol s	1.5	6.2
Transfer	$k_{fm_{11}}(j)$	L/kmol s	0.0021	0.0021
	$k_{fm_{12}}(j)$	L/kmol s	0.006	0.11
	$k_{fm_{21}}(j)$	L/kmol s	0.0021	0.001
	$k_{fm_{22}}(j)$	L/kmol s	0.006	0.11
	$k_{fh_1}(j)$	L/kmol s	0.088	0.37
	$k_{fh_2}(j)$	L/kmol s	0.088	0.37
	$k_{fr_1}(j)$	L/kmol s	0.024	0.12
	$k_{fr_2}(j)$	L/kmol s	0.048	0.24
	$k_{fs_1}(j)$	L/kmol s	0.0001	0.0001
	$k_{fs_2}(j)$	L/kmol s	0.0001	0.0001
Deactivation	$k_{ds}(j)$	s^{-1}	0.0001	0.0001
	$k_{dI}(j)$	L/kmol s	2000	2000
Impurity	$k_a(j)$	s^{-1}	0.0003	0.0003

Table 4

Table 4: Hydrodynamic equations used in the model

Parameter	Formula	Reference
Minimum fluidization velocity	$\mathrm{Re_{mf}} = [29.5^2 + 0.375\mathrm{Ar}]^{0.5} - 29.5$	[26]
Bubble velocity	$\mathrm{U_b} = \mathrm{U_0} - \mathrm{U_{mf}} + \mathrm{U_{br}}$	[27]
Bubble rise velocity	$\mathrm{U_{br}} = 0.711(\mathrm{g d_b})^{0.5}$	[27]
Emulsion velocity	$\mathrm{U_e} = \frac{\mathrm{U_0} - \mathrm{U_b}}{(1-\delta)}$	[28]
Bubble diameter	$\mathrm{d_b} = \mathrm{d_{b0}}[1 + 27(\mathrm{U_0} - \mathrm{U_e}]^{0.33}(1 + 6.84\mathrm{H})\ \mathrm{d_{b0}} = 0.0085$ (for GeldartB)	[29]
Mass transfer coefficient	$\mathrm{k_{be}} = \left(\frac{1}{\mathrm{k_{bc}}} + \frac{1}{\mathrm{k_{ce}}}\right)^{-1}$	
	$\mathrm{K_{bc}} = 4.5\left(\frac{\mathrm{U_e}}{\mathrm{d_b}}\right) + 5.85\left(\frac{\mathrm{D_g^{0.5} g^{0.25}}}{\mathrm{d_b^{1.25}}}\right)$	[27]
	$\mathrm{K_{ce}} = 6.77\left(\frac{\mathrm{D_g \varepsilon_e U_{br}}}{\mathrm{d_b}}\right)$	
Heat transfer coefficient	$\mathrm{H_{be}} = \left(\frac{1}{\mathrm{H_{bc}}} + \frac{1}{\mathrm{H_{ce}}}\right)^{-1}$	
	$\mathrm{H_{bc}} = 4.5\left(\frac{\mathrm{U_e \rho_g C_{pg}}}{\mathrm{d_b}}\right) + 5.85\frac{\left(\mathrm{k_g \rho_g C_{pg}}\right)^{0.5}\mathrm{g}^{0.25}}{\mathrm{d_b^{1.25}}}$	[27]
	$\mathrm{H_{ce}} = 6.77\left(\mathrm{\rho_g C_{pg} k_g}\right)^{0.5}\left(\frac{\mathrm{\varepsilon_e U_{br}}}{3}\right)^{0.5}$	
Bubble phase fraction Emulsion	$\delta = 0.534\left[1 - \exp\left(\frac{\mathrm{U_0} - \mathrm{U_{mf}}}{0.413}\right)\right]$	[30]
Emulsion phase porosity	$\varepsilon_\mathrm{e} = \varepsilon_\mathrm{mf} + 0.2 - 0.059\exp\left(-\frac{\mathrm{U_0} - \mathrm{U_{mf}}}{0.429}\right)$	[30]
Bubble phase porosity	$\varepsilon_\mathrm{b} = 1 - 0.146\exp\left(-\frac{\mathrm{U_0} - \mathrm{U_{mf}}}{4.439}\right)$	[30]
Volume of polymer phase in the emulsion phase	$\mathrm{V_{Pe}} = \mathrm{AH}(1 - \varepsilon_\mathrm{e})(1 - \delta)$	[22]
Volume of polymer phase in the bubble phase	$\mathrm{V_{Pb}} = \mathrm{AH}(1 - \varepsilon_\mathrm{b})\delta$	[22]
Volume of the emulsion phase	$\mathrm{V_e} = \mathrm{A}(1 - \delta)\mathrm{H}$	[22]
Volume of the bubble phase	$\mathrm{V_b} = \mathrm{A}\delta\mathrm{H}$	[22]

Table 5

Table 5: Operating conditions for petrochemical complex 1

Parameter	BP LL0209	BP HD3840	BP HD5218	BP HD6070
D_t(m)	4.8	4.8	4.8	4.8
H(m)	14.5	14.5	14.5	14.5
d_p(μm)	1145	1049	1061	965
T(°C)	317	310	313	316
P(bar)	20	19.91	19.85	19.99
U_0(m/s)	0.57	0.56	0.54	0.55
Ethylene concentration (%)	40	40	40	34
1-Butene concentration (%)	17	6.43	2.36	0.34
Hydrogen concentration (%)	9	16	30	23.46
Nitrogen concentration (%)	34	37.57	27.64	42.2
Catalyst feed rate (g/s)	0.2	0.2	0.2	0.2

Table 6

Table 6: Operating conditions for petrochemical complex 2

Parameter	BP LL0209													
Time	8:00	8:30	9:00	9:30	10:00	10:30	11:00	11:30	12:00	12:30	13:00	13:30	14:00	14:30
H (m)	19.76	19.77	19.74	19.79	19.87	19.87	19.83	19.6	19.91	20.12	20.13	20.04	20.11	20.12
d_p (μm)	986	986	986	986	986	986	986	986	986	986	986	986	986	986
P (bar)	21.8	21.81	21.81	21.8	21.83	21.79	21.81	21.81	21.74	21.74	21.73	21.77	21.75	21.76
U_0 (m/s)	0.634	0.635	0.636	0.635	0.635	0.633	0.634	0.633	0.634	0.634	0.631	0.629	0.631	0.632
Ethylene (%)	37.07	36.9	36.88	36.95	37.02	36.96	36.8	36.67	36.63	36.6	36.44	36.54	36.45	36.46
1-Butene (%)	13.73	13.75	13.73	13.71	13.69	13.67	13.63	13.64	13.55	13.55	13.57	13.54	13.56	13.57
Hydrogen (%)	4.57	4.58	4.62	4.62	4.6	4.6	4.65	4.65	4.63	4.65	4.69	4.66	4.69	4.68
Inert gas (%)	36.39	36.4	36.32	36.38	36.47	36.32	36.41	36.38	36.42	36.49	36.7	36.57	36.7	36.7
Catalyst feed rate (g/s)	0.661	0.661	0.661	0.661	0.661	0.661	0.661	0.661	0.661	0.661	0.661	0.661	0.661	0.661

Figure 2

Click here to download Supplementary MATLAB .fig files: fig02.fig

Figure 3

Click here to download Supplementary MATLAB .fig files: fig03.fig

Figure 4

Click here to download Supplementary MATLAB .fig files: fig04.fig

Figure 5

Click here to download Supplementary MATLAB .fig files: fig05.fig

Figure 6

Click here to download Supplementary MATLAB .fig files: fig06.fig

Figure 7

Click here to download Supplementary MATLAB .fig files: fig07.fig

Figure 8

Click here to download Supplementary MATLAB .fig files: fig08.fig

Figure 9

Click here to download Supplementary MATLAB .fig files: fig09.fig

Figure 10

Click here to download Supplementary MATLAB .fig files: fig10.fig

Figure 11

Click here to download Supplementary MATLAB .fig files: fig11.fig